High-sensitivity interferometric sensors on Si_3N_4 platform using Surface Plasmon Polariton (SPP)-based transducers

A. Manolis[1], E. Chatzianagnostou[1], G. Dabos[1], N. Pleros[1], B. Chmielak[2], A.L. Giesecke[2], C. Porschatis[2], P. J. Cegielski[2], L. Markey[3], J.C. Weeber[3], A. Dereux[3] and D. Tsiokos[1,4]

[1] Department of Informatics - Center for Interdisciplinary Research and Innovation, Aristotle University of Thessaloniki, Greece

[2] AMO GmbH, Advanced Microelectronic Center Aachen (AMICA), Otto-Blumenthal-Strasse, Aachen, Germany

[3] Laboratoire Interdisciplinaire Carnot de Bourgogne, CNRS-Université de Bourgogne, Dijon, France

[4] bialoom Ltd, 72, 28th Octovriou Avenue, Office 301, Engomi, 2414 Nicosia, Cyprus

e-mail: athanasm@csd.auth.gr

ABSTRACT

In this work, we report an interferometric plasmo-photonic sensor based on Si_3N_4 photonic waveguides and gold (Au) Surface Plasmon Polariton (SPP) stripe waveguides. The proposed approach exhibits bulk sensitivity up to 1930 nm/RIU, holding promise for compact, ultra-sensitive interferometric sensing devices. We also evince experimentally that the proposed plasmo-photonic waveguide employed at the interferometer sensing arm can be fabricated using Aluminum (Al) instead of gold, demonstrating the first step towards fully CMOS compatible plasmo-photonic interferometric sensors.

Keywords: refractive index sensor, plasmonic stripes, silicon nitride, photonic integrated circuits, CMOS metals.

1. INTRODUCTION

Plasmonic-based sensors have emerged as an attractive sensing technology for point of care applications. Compared to the evanescent wave photonic sensors, plasmonic sensors offer profound exposure of SPP modes to liquid analytes leading to enhanced sensitivity characteristics [1]. However, bulky prism-based coupling configurations [2] and high plasmonic losses [3] impede the transfer of those benefits in miniaturized and multi-functional all-plasmonic sensors. As an alternative, selective co-integration of plasmonic waveguides in low loss photonic platforms addresses those challenges while leveraging the functional benefits from both waveguide platforms [4]. In this work, we demonstrate a photonic integrated Mach-Zehnder interferometric sensor utilizing an open cladded gold stripe in one branch to serve as the sensing transducer by detecting local changes in the refractive index. The low-loss Si_3N_4 platform allows for the deployment of a MZI-based variable optical attenuator (VOA) followed by a thermo-optic phase shifter in the reference branch, in order to optimize the sensor performance. The proposed sensor was designed, fabricated and experimentally characterized, yielding bulk sensitivity values up to 1930 nm/RIU, demonstrating the functional benefits of the co-integration of plasmonic and photonic waveguides. We also evince through experimental data the dependence of bulk sensitivity from the Free Spectral Range (FSR), suggesting an effective roadmap towards compact and ultra-sensitive interferometric sensors. Following the successful demonstration of the plasmo-photonic sensor utilizing a gold stripe, we evince experimentally that the proposed plasmo-photonic waveguide employed at the interferometer sensing arm can be fabricated using Aluminum (Al) instead of gold, demonstrating the first step towards fully CMOS compatible plasmo-photonic interferometric sensors. The CMOS structures were fabricated and experimentally characterized, demonstrating Si_3N_4 to Al stripe interface loss equal to 2.86 dB and propagation losses of 0.065 dB/μm at 1550 nm, which is, to the best of our knowledge, the lowest SPP propagation losses among all single-mode Al-based plasmonic waveguides demonstrated so far at 1550 nm, reducing the propagation losses reported in our previous work [5].

2. PLASMO-PHOTONIC SENSOR

2.1 Layout and fabrication

Fig. 1(a) illustrates a schematic of the proposed plasmo-photonic sensor layout. The different cross-sections across the structure including the photonic waveguide (I), the taper end facet (II), the plasmonic waveguide (II) and the thermo-optic phase shifter (IV) are depicted in Fig. 1(b). The photonic waveguide platform relies on a 360 nm × 800 nm Si_3N_4 photonic waveguide core cladded with 600nm of Low Temperature Oxide (LTO) while relying on a 2.2 μm thick SiO_2 substrate layer (Fig.1(b)(1)). The sensing branch exploits a butt-coupling mechanism, comprised of a 100 nm × 7 μm Au SPP waveguide interfaced at its both end facets with two 7.5 μm wide linearly tapered Si_3N_4 waveguides [6]. The reference branch comprises a thermo-optic heater-based phase shifter for tuning the sensor's resonance wavelengths and a VOA for counter balancing the high plasmonic optical losses on the sensing arm, eventually maximizing field interference at the MZI output and therefore the spectral extinction ratio.

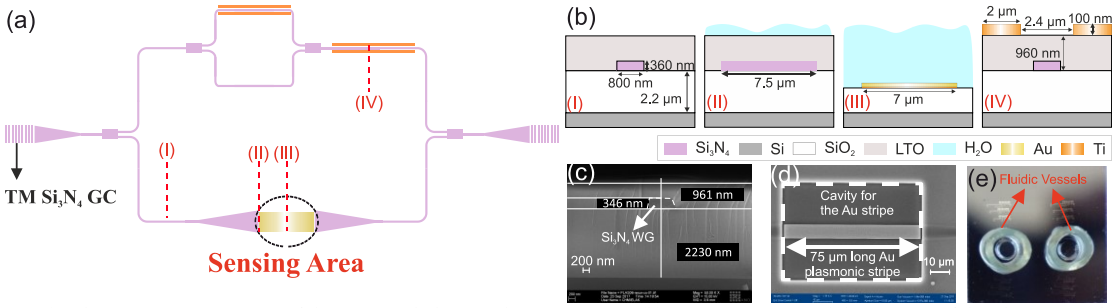

Figure 1. (a) Schematic representation of the proposed plasmo-photonic sensor. (b) Cross-sections and dimensions of the photonic and the plasmonic waveguides. (c) cross section SEM image of the photonic waveguide. (d) SEM top-view image of the gold plasmonic waveguide recessed in the cavity. (e) Photo of the fabricated sensor chip illustrating the fluidic tubes glued on top of the chip.

The phase shifter consists of two 100 nm × 2 μm titanium resistors, placed on top of the photonic waveguide, in a double-heater configuration ((Fig.1(b)(IV)). The VOA is composed of a MZI, with a thermo-optic heater-based phase shifter in one branch in order to control the attenuation of optical power with applied voltage. Moreover, two low-loss 3-dB Multi-Mode Interference (MMI) Y-junctions were utilized to allow equal power splitting ratios between the MZI branches. The fiber-to-chip coupling relied on a vertical out-of-plane coupling scheme based on Si_3N_4 Grating Couplers (GCs) for Transverse Magnetic (TM) polarization [7].

For the fabrication of the proposed plasmo-photonic sensor, a standard 6'' silicon wafer with 2.2 μm of thermally grown SiO_2 has been employed as substrate. The Si_3N_4 waveguide was deposited in low pressure chemical vapor deposition process (LPCVD). Marker layer and waveguides have been defined by optical projection lithography using an i-line stepper tool. Reactive-Ion-Etching (RIE) with CHF_3 and He chemistry has been employed for the structure transfer. Afterwards, a 600 nm thick LPCVD SiO_2 was deposited to form the LTO cladding of the photonic waveguide and annealed at 1000 °C for several hours. A Scanning Electron Microscope (SEM) image of a cross section view of the fabricated photonic waveguide is depicted in Fig. 1(c). The cavity for the plasmonic material were defined by the i-line stepper tool and etched through LTO, Si_3N_4 and SiO_2 as well by RIE with CHF_3 and He chemistry. In the final fabrication stage, the gold plasmonic stripes were deposited into the cavities by a lift-off process using e-beam lithography, thermal evaporation of gold and lift-off dissolution. The target thickness for gold was 100 nm. A very thin (3nm) titanium layer was deposited by e-gun evaporation prior to gold for an improved adhesion of gold on the sample. A SEM image of the fabricated plasmonic stripe is shown in Fig. 1(d). Silicone fluidic vessels were also glued on top of the plasmonic sensing waveguides as the means to confine the test liquid in this region alone, as shown in more detail in Fig. 1(e).

2.2 Experimental characterization

Characterization measurements were carried out to evaluate bulk sensitivity capabilities of the proposed plasmo-photonic sensor. In our measurements we tested two sensor variants with different Free Spectral Ranges (FSR) that were developed during the same process. Broadband measurements were carried out by sweeping the wavelength of a tunable laser source from 1500 nm to 1580 nm to launch light into the Si_3N_4 GCs. Moreover, voltage was applied to the titanium based heaters of the VOA in order to introduce additional losses in the reference branch as the means to maximize the extinction ratio on the output of the MZI sensor. The obtained FSR and the ER for sensor 1 were measured equal to 16 nm and 33.5 dB, respectively, while the corresponding values for sensor 2 were calculated equal to 24.8 nm and 37 dB, respectively. Sensitivity measurements were accomplished by infiltrating different buffer solutions with refractive indices ranging between 1.3327 and 1.3388 into the sensing area of each sensor. The respective spectral responses are indicatively illustrated in Fig 2(a) and 2(b), clearly revealing that the resonances are shifting to longer wavelengths with increasing refractive index of the buffer solution. Consequently, bulk sensitivity values were calculated by applying least-squares linear fitting on the resonant wavelength shift with increasing refractive index change, as shown in Fig. 2(c). Maximum bulk sensitivities were calculated 383 nm/RIU at 1527 nm and 1930 nm/RIU at 1565 nm for sensor 1 and 2, respectively. Experimental results showed that the sensor with the larger FSR exhibited also larger bulk sensitivity values, revealing the dependence of sensitivity with the FSR.

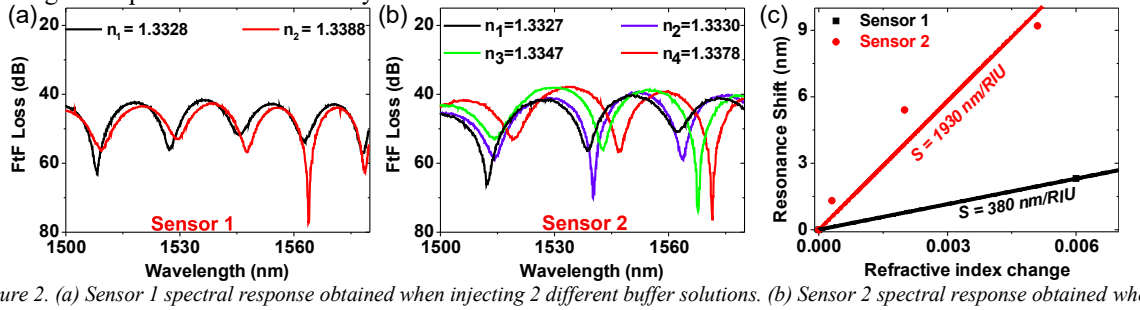

Figure 2. (a) Sensor 1 spectral response obtained when injecting 2 different buffer solutions. (b) Sensor 2 spectral response obtained when injecting 4 different buffer solutions. (c) Resonance shift versus refractive index change, illustrating linear fitting plots for each sensor.

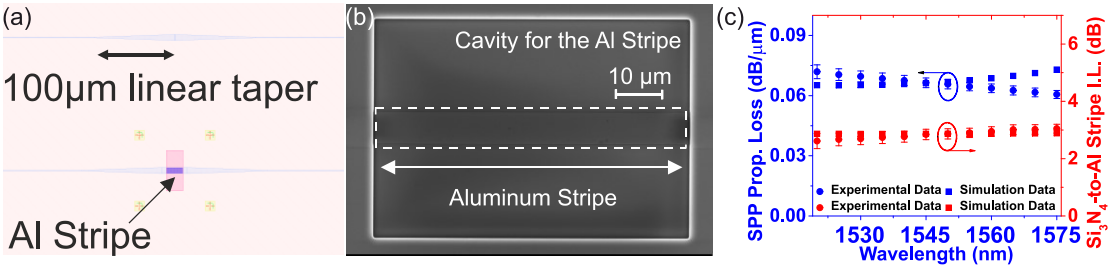

Figure 3. (a) Mask layout showing the reference waveguide and a Si_3N_4-to-Al interface test structure. (b) SEM image of the Al plasmonic stripe recessed in the cavity. (c) Broadband experimental data for the interface and propagation loss in water.

3. ALUMINUM STRIPES

The successful experimental results for the Au-based plasmo-photonic sensor motivated us to fabricate and test the proposed plasmo-photonic waveguide, employed at the interferometer sensing arm, on a separate chip, relying now on CMOS compatible plasmonic waveguides, by replacing gold with low cost Aluminum.

We evaluated the Al plasmonic waveguides in aqueous environment, by conducting broadband optical characterization based on Fiber-To-Fiber (FtF) measurements and following a standard cutback method. A highlight of the mask layout presenting the test structures that has been measured is shown in Fig. 3(a). The test structures included a reference waveguide and Si_3N_4-to-Al interface test structures with varied plasmonic stripe length (20, 50, 100, 150, 200 and 250 μm). The reference structure comprised of a 0.88 cm long straight Si_3N_4 waveguide with two 100 μm long linear tapers in the middle, interconnected to each other via 1 μm long and 7.5 μm wide waveguide. A SEM image of a 70 μm long Al stripe, recessed in the cavity between the Si_3N_4 waveguide facets, is shown in Fig. 3(b). The plasmonic propagation losses as function of wavelength have been obtained by performing a linear fitting process, based on least-squares method, to the experimental data. In order to calculate the Si_3N_4-to-Al interface loss, the losses of the reference Si_3N_4 waveguide structure were subtracted from the intercept values obtained by the fitting process and the resulting loss value was divided by a factor of two. Figure 3(c) presents the obtained characterization results for the plasmonic propagation losses and the interface loss as a function of wavelength, in comparison with the respective simulation results. Measurements dictated a plasmonic propagation loss of 0.065 dB/μm, which translates to a propagation length (Lspp) of 66.8 μm and a Si_3N_4-to-Al interface loss of 2.86 ± 0.07 dB at 1550 nm being in good agreement with the simulated values.

4. CONCLUSIONS

We demonstrate an interferometric sensor configuration, exploiting a gold based plasmo-photonic structure as the sensing element, achieving bulk sensitivity values up to 1930 nm/RIU. We also evince experimentally that the proposed plasmo-photonic waveguide employed at the interferometer sensing arm can be fabricated using Aluminum (Al) instead of gold, revealing an effective roadmap towards low-cost and CMOS-compatible integrated plasmo-photonic biosensors.

ACKNOWLEDGEMENTS

This work was supported by the European H2020 ICT PLASMOfab (no.688166) project. The authors would like to acknowledge Dr. Stefan Schrittwieser and Dr. Rudolf Heer from the Austrian Institute of Technology (AIT) for the fabrication and the adhesion of the silicone fluidic tubes on the sensor chip.

REFERENCES

[1] G. A. Lopez, M. Estevez, M. Soler, and L.M. Lechuga : Recent advances in nanoplasmonic biosensors: applications and lab-on-a-chip integration, *Nanophotonics,* vol. 6, pp. 123-136, 2017.

[2] J. Homola: Surface plasmon resonance sensors for detection of chemical and biological species, *Chem. Rev.* vol. 108, pp. 462–493, 2008.

[3] A. Khan, O. Krupin, E. Lisicka-Skrzek, and P. Berini: Mach-Zehnder refractometric sensor using long-range surface plasmon waveguides, *Appl. Phys. Lett.*, vol. 103(11), 111108, 2013

[4] X. Sun, D. Dai, L. Thylén, and L. Wosinski: High-sensitivity liquid refractive-index sensor based on a Mach-Zehnder interferometer with a double-slot hybrid plasmonic waveguide, *Opt. Express*, vol. 23, pp. 25688-25699, 2015.

[5] G. Dabos *et al.*: Aluminum plasmonic waveguides co-integrated with Si_3N_4 photonics using CMOS processes, *Scientific Reports*, vol. 8, no. 1, art. no. 13380, 2018.

[6] G. Dabos *et al.*: Plasmonic Stripes in Aqueous Environment Co-Integrated With Si3N4 Photonics, *Photonics Journal*, vol. 10, pp. 1–8, 2018.

[7] G. Dabos *et al.*: TM grating coupler on low-loss LPCVD based Si_3N_4 waveguide platform, *Opt. Commun.*, vol. 405, pp. 35–38, 2017.